Pergamon

Int. J. Heat Mass Transfer. Vol. 41, Nos 8–9, pp. 1049–1063, 1998

Printed in Great Britain
0017–9310/98 $19.00+0.00

PII: S0017–9310(97)00181–6

Developing turbulent mixed convection in a horizontal circular tube with strip-type inserts

SHOU-SHING HSIEH, MING-HO LIU and FENG-YU WU

Department of Mechanical Engineering, National Sun Yat-Sen University, Koashiung, Taiwan 80424, Republic of China

(*Received* 22 *January* 1997 *and in final form* 7 *June* 1997)

Abstract—An experimental study was undertaken for developing turbulent mixed convection in a horizontal circular tube with strip-type inserts (longitudinal strip LS and crossed-strip CS inserts) for $6500 \leqslant Re \leqslant 19{,}500$ and $5.82 \times 10^4 \leqslant Gr^* \leqslant 9.78 \times 10^7$. Temperature data were measured and heat transfer rates at different heat flux levels were calculated and correlated in the form of relevant parameters. The buoyancy effect was detailedly examined for $1.53 \times 10^{-4} \leqslant Gr^*/Re^2 \leqslant 2.31$. It is found that the buoyancy effect has less influence for tubes with inserts compared to the bare tubes. Moreover, the heat transfer enhancement was found 2–3 times than those of bare tubes. © 1997 Elsevier Science Ltd.

INTRODUCTION

Combined free and forced convection in the tube entrance region has many diverse industrial and engineering applications, such as heat exchangers and chemical processes. It is long recognized that gravity plays an important role in characterizing mixed convection duct flows. If the orientation of the duct is not vertical, the buoyancy force induces the secondary flow, which enhances heat transfer between the wall and the fluid. Such effects are most pronounced in horizontal flows and there have been numerous studies for various enclosure shapes and thermal boundary conditions. A number of studies in the literature have been on laminar convection in a horizontal smooth duct with buoyancy effect [1]. In spite of this, mixed convection with weak buoyancy is also observed for $Gr^*/Re^2 < 50$ in turbulent flow.

As a practically used displaceable device, a longitudinal rectangular plate is often inserted in tubes of heat exchangers to enhance tubeside heat transfer. Recently, Solanki *et al.* [2, 3] conducted experimental and theoretical studies on laminar forced convection in tubes with polygonal inner cores. Chen and Hsieh [4] numerically studied laminar mixed convection in a horizontal tube with a longitudinal square core.

Most studies were concerned with fully developed conditions. However, it was unclear how the flow develops to the final states for turbulent mixed convection in a horizontal tube, especially with a longitudinal strip in its core. The developing process would not only provide insight into the complicated physics involved, but also legitimize the fully developed solution. Most recently, Hsieh and Wen [5] made another numerical study for the same topic under developing entrance flow condition. However, literature on developing three-dimensional (3-D) turbulent mixed convection tube flow with a longitudinal insert is relatively scare. The purpose of the present work is to extend the previous studies [4, 5] of the developing turbulent tube flow and heat transfer with strip inserts and to examine the thermal effect on forced convection in this type of turbulent flow. The geometry and dimensions of the insert used in this study is shown in Fig. 1 which were chosen to meet the applications in waste heat recovery system as a recuperator. The insert was made from plexiglas and considered as adiabatic.

EXPERIMENTAL APPARATUS AND PROCEDURE

The open air flow loop is similar to that used in two earlier studies [5, 6]. It consists of a double tube structure with four different strip type inserts of isoflux peripherally heated, a calibrated orifice flow meter, a flow straightener, an entrance section, and the test section. The geometry, coordinate system, boundary conditions and the details of the experimental apparatus are similar to the one in ref. [6]. The test section is a straight, circular tube made of stainless steel. The tube wall of the test section is heated uniformly with an electric heater, the power input to each heater being controlled with a variable transformer. The data to be presented are for air ($Pr \sim 0.7$) with approximate power input of 685, 1370 and 2055 W. The inner tube of the heating part which is the test tube of $D = 58$ mm is made of 4 mm-thick aluminum plate. The test circular tube is $D = 110$ mm and 3000 mm in length. Figure 2 presents a schematic of the apparatus and instrumentation. The heating element was a sandwich type heater of 18 mm diameter into a quartz made

NOMENCLATURE

AR	aspect ratio, L/H
A	heat transfer area
C_p	specific heat at constant pressure
D	tube inner diameter, also tube hydraulic diameter
g	gravity
Gr^*	modified Grashof number, $g\beta D^4 q''/v^2 k_f$
H	height of insert
h	heat transfer coefficient
k_f	thermal conductivity of air at film temperature
L	width of insert
ℓ	length of the test tube
Nu	Nusselt number, hD/k_f
Pr	Prandtl number, v/α
Q_{net}	net convection heat flow rate
Q	the total heat input to the test section
q''	heat flux, Q_{net}/A
R	radius of inner tube
Re	Reynolds number based on hydraulic diameter, VD/v
T	temperature
V	bulk average velocity
x, y	rectangular coordinates.

Greek symbols

α	thermal diffusivity
β	thermal expansion coefficient
v	kinematic viscosity
ρ	density of working fluid.

Subscripts

BR	bare tube
b	bulk
CS	crossed-strip type inserts
F	forced convection
f	fluid
in	inlet
LS	longitudinal strip-type inserts
m	mixed convection
N	natural convection
out	outlet
w	wall
x	local position in the main flow direction.

Superscripts

+	dimensionless
–	average.

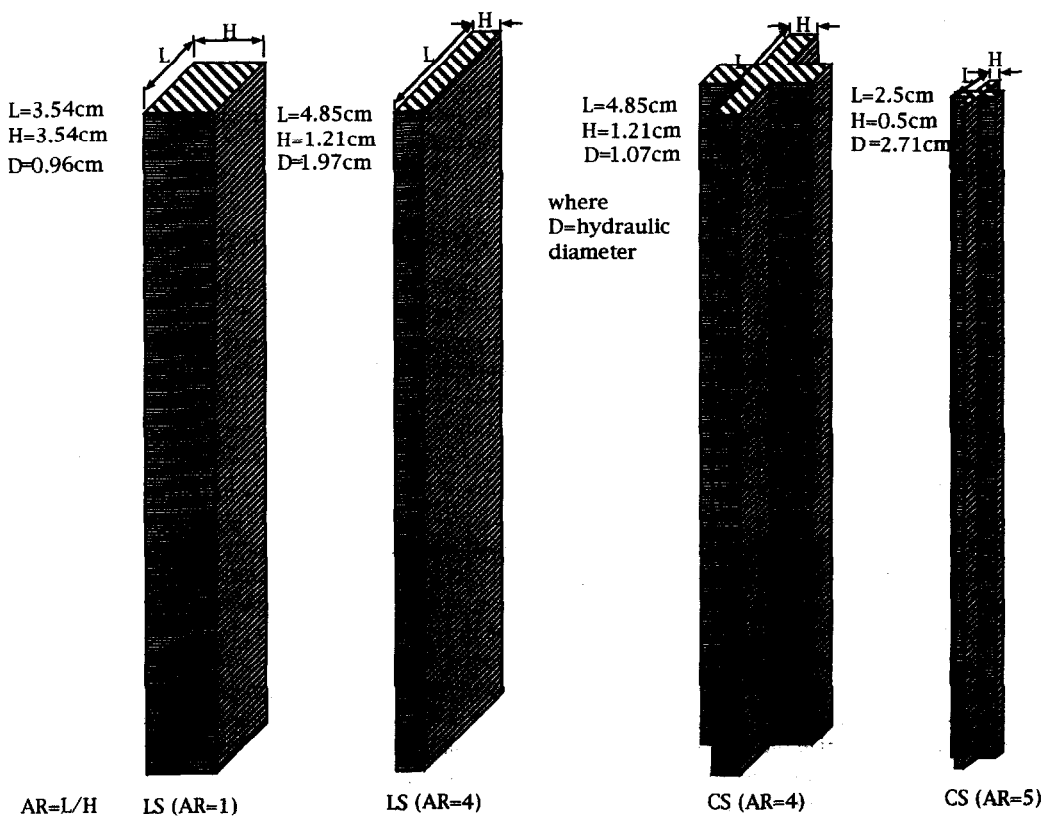

Fig. 1. The geometry and dimensions of the insert considered in the present study.

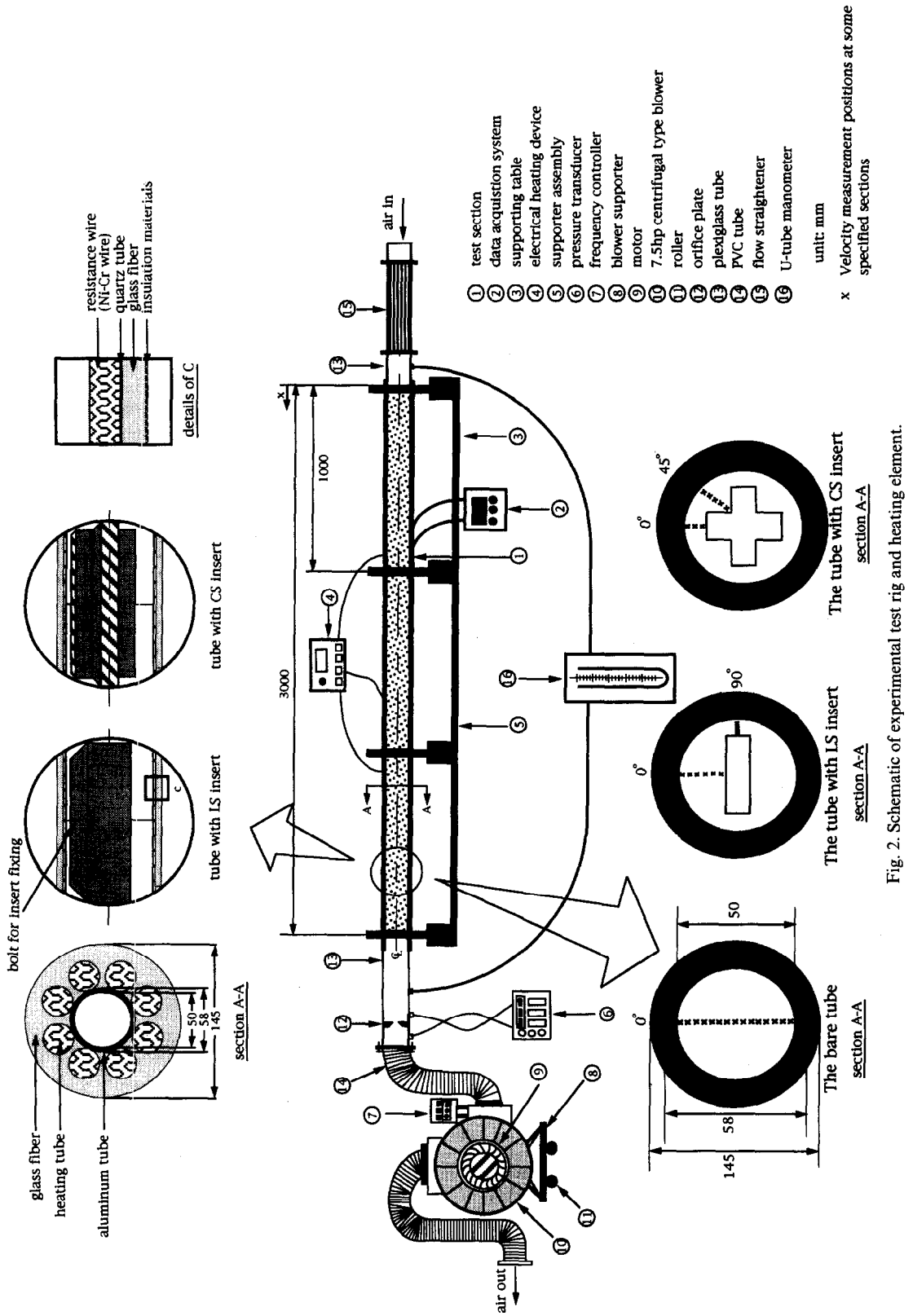

Fig. 2. Schematic of experimental test rig and heating element.

shield which is also shown in Fig. 2 and was designed to provide uniform power dissipation per unit length. It comprises a nickel–chromium wire (gage 1.8 mm dia.) wound over the glass wool at 120 windings m^{-1}. The heating element was placed inside the outer tube, and the annular space between the two was filled with electrical Meca and cement.

All measurements were made with air as the fluid. The locations of the thermocouples used to measure the tube wall temperature distribution were described in ref. [6] and were also shown in Fig. 3. The thermocouples were installed in holes drilled into the back side of the test tube walls to within ± 2 mm of the tube surface. Thirty 24-gage copper–constantan thermocouples were installed along the axial centerlines of the tube. The detailed measurement positions were also shown in Fig. 3. Five thermocouples, positioned just up/down stream of the tube inlet/exit, were used to measure the entering/exiting bulk temperatures. The thermocouple voltage outputs were fed into an OMEGA μR-100 scanning data logger which had the capability to time-average the output. Electric power was supplied to the test section heating wire by one independent circuit. The source of power for the circuit was an autotransformer, supplied from a standard 220 V 60 cycle a.c. wall outlet. These autotransformers were designed for a load voltage output of 0–220 V with a maximum current of 10 amps. The voltage drops across the resistance wire and across one shunt resistors were converged to a multimeter. The room air was drawn into the channel entrance over the heated test section to a downstream blower, which was operated in suction mode.

Mass flow rate of the air was determined from the measured pressure drop across an orifice plate. The orifice meter was calibrated by measuring the velocity profile in the tube in which the meter was installed by a hot wire anemometer. The flow meters have a calibrated accuracy of 5 percent. The air supply to the experimental apparatus was giving a range of Reynolds numbers of 6500–19,500 based on the hydraulic diameter D and nominal average velocity V. Corresponding Gr^*/Re^2 range from 1.53×10^{-4} to 2.31. The present experiments will give us the total heat transfer, Q, where Q at the steady state is the sum of Q_{net} due to convection, the radiation heat loss Q_r, and the conduction heat loss, Q_c. Therefore,

$$Q_{net} = Q - Q_r - Q_c \tag{1}$$

The radiation heat loss and the conduction heat loss were found approximately 5 and 3%, respectively, of the input power. The local total heat transfer coefficients $h_{x,t}$ would be obtained as follows:

$$h_{x,t} = \frac{Q_{net}}{A(T_{w,x} - T_{b,x})}. \tag{2}$$

To prepare the test apparatus for a set of experiments, the inserts used in the previous set of experiments are removed and the interior surface of the test section are cleaned thoroughly with an adhesive solvent. The inserts for the experiments are then installed. Extreme care is taken to position the insert segments accurately and to ensure good contact. After the test section is reassembled, the blower is switched on to allow air to flow through the test channel and a solution of soap and water is used to check for air leakage. To initiate an experiment, air at a predetermined mass flow rate is allowed to flow through the test tube.

Energy balances are used to determine $T_{b,x}$, the local bulk mean temperature at any streamwise tube location in equation (2). The form of the energy equation used for this purpose is given by:

$$T_{b,x} = T_{b,i} + \left(\frac{Q_{net}}{\pi D \ell}\right) \times \left(\frac{\pi D \Delta x}{m C_p}\right) \tag{3}$$

where Δx is the stream distance from the beginning of heating for the streamwise station of interest, m is the air mass flow rate and C_p is air specific heat.

Power is then supplied to the heaters to maintain the wall temperatures near the exit about ± 0.1°C above the exit air temperature to avoid the heat transfer from the surroundings. Steady-state is reached in 2 h. The heater voltages and currents along with all temperatures are then recorded. The maximum variations of some of the readings are recorded for the uncertainty analysis of the results. The barometric pressure is read at the beginning and the end of a test run. In separate no-flow experiments, a correlation between the rate of heat loss through the fiberglass insulation and the average wall temperature is made. A qualification test for mass and energy balance as stated earlier was also made for each test run.

EXPERIMENTAL UNCERTAINTY

An error analysis using the method of Moffat [7] was performed to determine the uncertainty in the experimental data. The single largest contributor to uncertainty in the Reynolds number was the measurement of the volumetric flow rate. The resulting maximum uncertainty in Re is 8.2%. The majority of the error in Nu can be traced to the uncertainty in the convective heat transfer and temperature difference. The uncertainty in convective heat transfer is due mainly to the simplified analysis for the conduction loss correction. Although the conduction loss through the insert considered as adiabatic can probably be estimated only to within 2 and 3% accuracy, these losses are so small that it might be negligible. The estimated error in the temperature difference 0.2°C. Temperature differences were ranged from 20°C to a maximum of 60°C. The resulting maximum uncertainty in Nu is 8%.

RESULTS AND DISCUSSION

The present study was conducted for $Q = 685$, 1370 and 2055 W with the atmospheric air as the convective

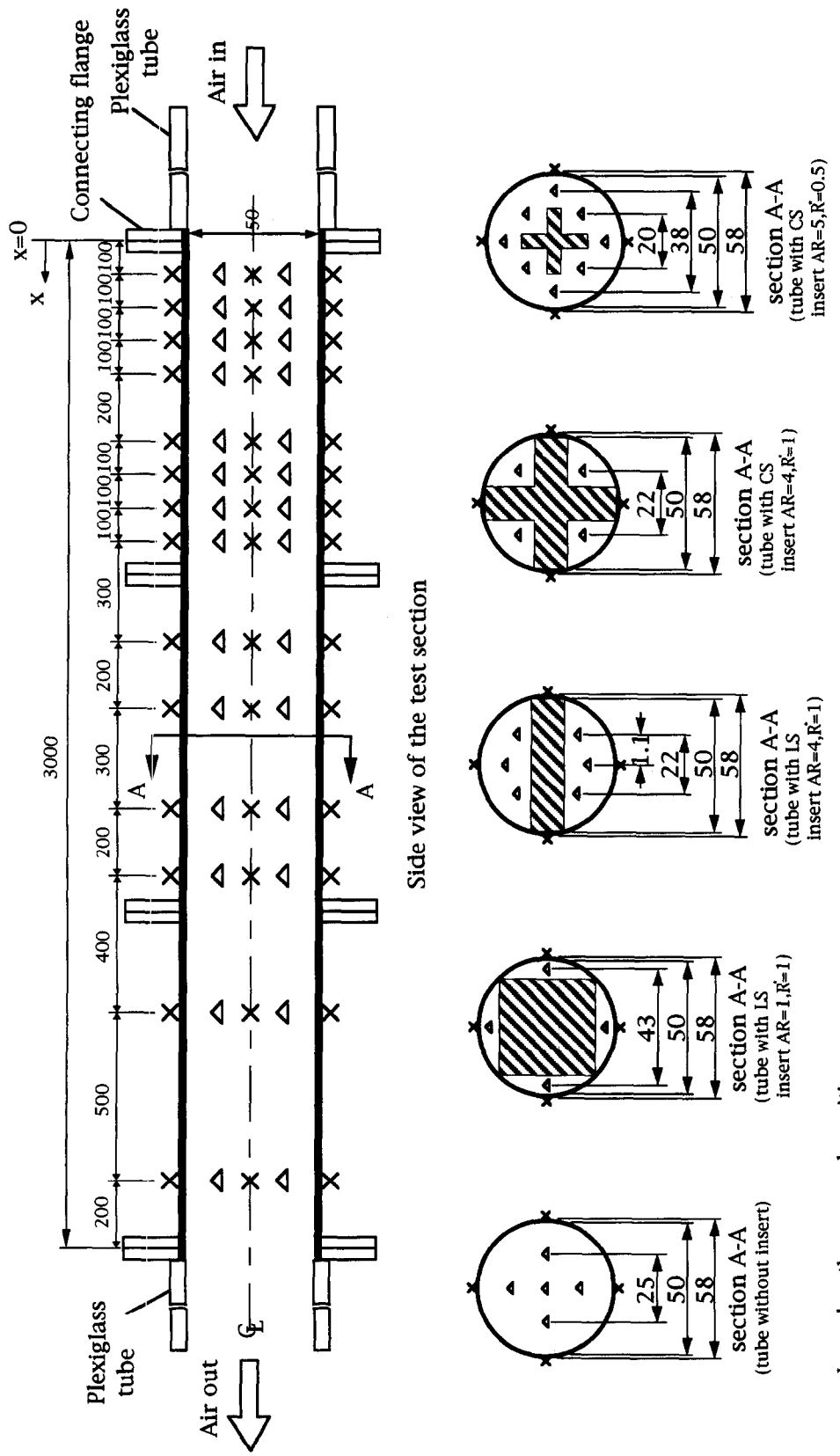

Fig. 3. Thermocouple measuring position for temperature measurements.

medium. The range of Gr^*/Re^2 varied from 1.53×10^{-4} to 2.31. The velocity (bulk averaged) level for the present study was about 2.03–28.63 m s^{-1}.

The determination of fully-developed Nusselt numbers from the experimental data began with the calculation of the overall bulk temperature rise based on an energy balance on the flowing air. The slope of this temperature rise was then obtained by dividing by the heated length of the test tube. A plot of the measured test tube wall temperature was then prepared in order to determine the range over which the slope of the wall temperature was equal to the calculated bulk temperature slope, indicating the region of fully-developed heat transfer. A representative temperature distribution for five tubes tested at $Gr^*/Re^2 = 0.254$ at $Re = 16{,}250$ as shown in Fig. 4. This also verifies the present experimental procedure.

The most important portion of this figure is the central segment through which a straight line has been fitted to the line representing the fluid bulk temperature. The vertical distance between this line segment and the bulk-temperature line indicates the wall-to-bulk temperature difference used in calculating the fully developed heat-transfer coefficient. It is found that the smallest temperature difference exists for LS insert with $AR = 1$ and CS insert with $AR = 4$. Both found having the thermal entrance length about $4D$. While the largest temperature difference happens for the bare tube. The departure of the wall temperature data from straight line behavior at upstream end of the test tube was due primarily to the absence of front-side heating at this end. Flow development at upstream end seems dominant for the cases of bare tube and LS insert with $AR = 4$ and CS insert with

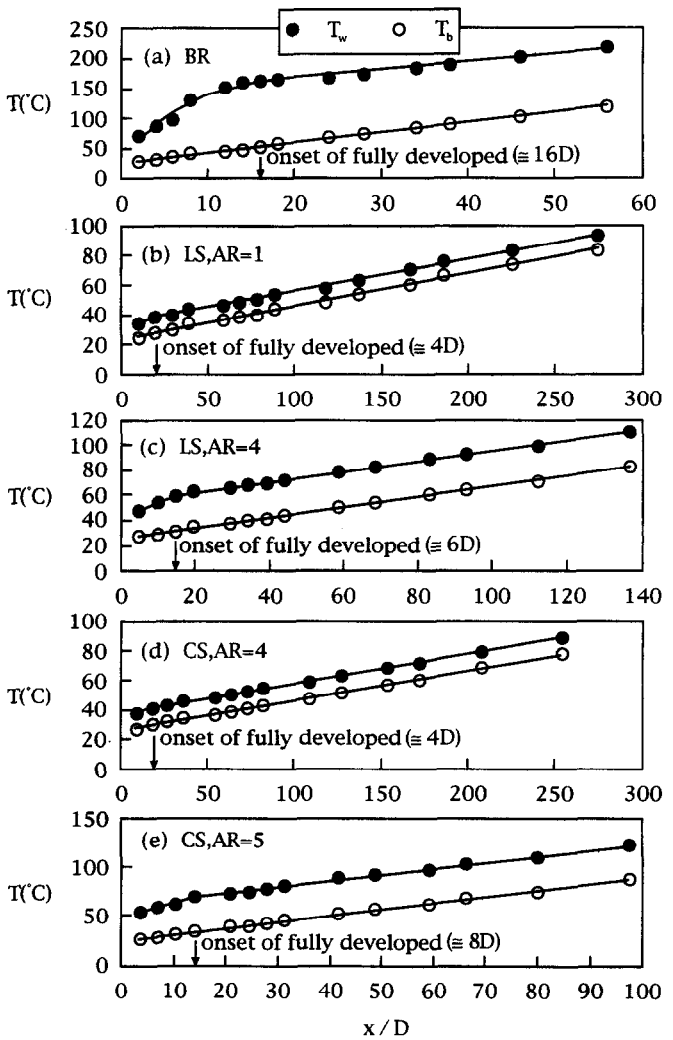

Fig. 4. The variations of tube wall and bulk fluid temperature along x/D at $Gr^*/Re^2 = 0.254$ and $Re = 16{,}250$ for different tubes with/without insert.

Table 1. Thermal entrance length correlations

Tube	Correlations ($Pr = 0.7$)
Bare	$L_e/D = 5.05Re^{0.168}Pr^{0.158}$
LS ($AR = 1$)	$L_e/D = 1.11Re^{0.148}Pr^{0.158}$
LS ($AR = 4$)	$L_e/D = 1.98Re^{0.157}Pr^{0.158}$
CS ($AR = 4$)	$L_e/D = 1.15Re^{0.150}Pr^{0.158}$
CS ($AR = 5$)	$L_e/D = 2.58Re^{0.163}Pr^{0.158}$

$AR = 5$. Detailed correlations of L_e/D vs Re and Pr for thermal entrance length were tubulated in Table 1. Since the working fluid is air and the value was considered as constant ($= 0.7$), the exponent for Pr was chosen as the same as that for Re.

The developing process can be illustrated from heat transfer distribution along the downstream distance. Figure 5 shows the results from bare tube at two different Reynolds numbers for three different heat flux levels and indicates the heat transfer in the cross-section is enhanced by the secondary flow due to buoyancy. The local Nusselt number does not rise immediately, however, because the flowing thermal boundary layer impedes the heat transfer. The balance between these two effects is reached at $x/D \cong 10$ at $Re = 6500$ in which $0.95 \leqslant Gr^*/Re^2 \leqslant 2.31$ and hence occurs the minimum of Nu in Fig. 5(a). This is also the point ($x/D \cong 13$) when the Nusselt number starts to deviate from the forced convection values from [6] in Fig. 5(a). As Re increased to 19,500 as shown in Fig. 5(b), secondary flow orthogonal to the forced flow can be much less prominent and effective. Moreover, at this stage, it suggests that the axial velocity exhibits predominantly forced convection flow behavior. Actually, the values from pure forced convection are a little different from the present results for mixed convection in the beginning of the flow. This is because the entry

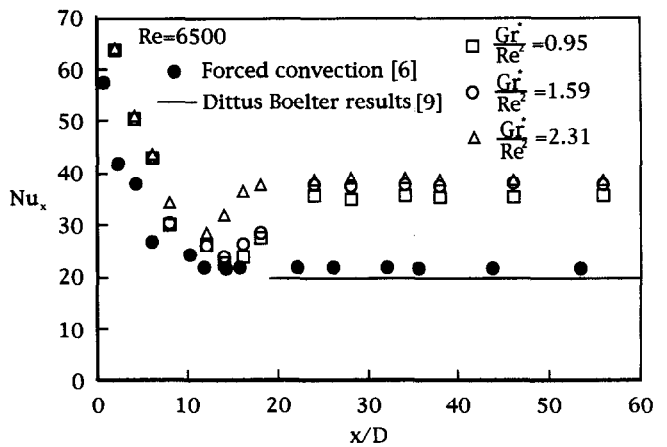

(a)

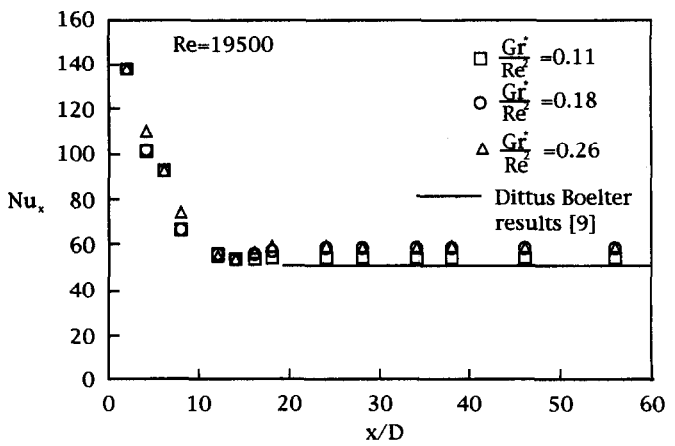

(b)

Fig. 5. Local Nusselt number variations along x/D under different heat flux level at: (a) $Re = 6500$; (b) $Re = 19{,}500$ for bare tube.

region boundary layers at $Re = 6500$ could be laminar like or less fully developed when $x/D \leqslant 12$. A similar phenomenon was also observed and discussed in Choi and Choi [8] in mixed convection flow in a horizontal tube.

Furthermore, the developing process at $Re = 6500$ shown in Fig. 5(a) indicates that the secondary motion due to buoyancy in this case is much stronger than that of Fig. 5(b) at $Re = 19{,}500$, which is expected. The fact that the secondary flow is most intense at this axial location (i.e. $x/D \leqslant 20$) and causes the Nusselt number to have their maximum values at this location at $Re = 6500$ where $0.95 \leqslant Gr^*/Re^2 \leqslant 2.31$. Farther downstream, at $x/D > 20$, the secondary flow becomes weaker due to the disappearance of natural convection effects. At sufficiently far downstream locations, the secondary flow disappears altogether as the fluid reaches wall temperature and the flow becomes fully developed which can be seen in Fig. 5. This was evidenced by flow visualization reported from [5] for laminar flow. *Nu* data in Fig. 5 show a systematic increase with increasing Gr^*/Re^2, but this is not clearly noted for $Re = 19{,}500$. This was further confirmed in the later section in Fig. 10. This is obvious because the present buoyancy assists the forced flow at $Re = 6500$ more than that at $Re = 19{,}500$. Because the *Nu* increases with Gr^*/Re^2 in the present study occur at all x/D, the qualitative character of the changes are the same regardless of thermal boundary layer development. Regions where *Nu* decreases with x/D in Fig. 5 are regions where the tube thermal boundary layer are less than fully developed. At a particular Gr^*/Re^2 (say $\cong 0.11$) at $Re = 19{,}500$, this occurs at $x/D \leqslant 15$. Also shown in Fig. 5(b) is the results from Dittus and Boelter [9], comparisons show that fully developed values from the present study at $Re = 19{,}500$ match at downstream locations except that the values of present study show a little bit higher than the Dittus and Boelter's due to thermal buoyancy. The buoyancy induced motions in this situation may thus locally augment advection very near tube surface giving mixed convection *Nu* which may be locally higher than *Nu* values of pure forced convection especially at a low Re ($=6500$).

Near the inlet, the buoyancy force is yet to be developed as stated earlier in Fig. 5 and all the curves follow that of the forced convection flow. As x/D increases, however, the buoyancy effects become noticeable and each curve again shown in Fig. 6 starts to deviate from the limiting curve. The situation becomes more evident as Q increases and when Re is small. The enhanced effect due to present flow and heating condition can be clearly observed. The reasons can be explained as follows: the buoyancy force induces secondary flow and the resulting mixing increases the flow resistance and the heat transfer between the wall and the fluid.

The developing thermal boundary layers ($x/D \leqslant 16$) can also be noted and one contained mostly within the low Re portion (e.g. $Re = 6500$) of the momentum boundary layer where buoyancy induced motions have at least equivalent magnitudes (see Gr^*/Re^2 for details). Furthermore, such buoyancy induced secondary flows enhance *Nu* over pure forced convection values in tubes. This is more obvious in tubes especially for large heat inputs and low Reynolds numbers which can be seen from Fig. 6.

When tube thermal layers merge to become fully developed ($x/D > 16$), Fig. 6 shows that buoyancy induced motions augment Nusselt numbers compared to pure forced convection values. At a particular x/D, *Nu* increases continuously as Re decreases (i.e. Gr increases relatively). Velocities induced by natural convection with this situation are generally significantly competent with that streamwise advection velocities associated with the forced flow. Thus, the effect of the buoyant motions is to enhance the forced velocities and accelerate the flow especially near tube surfaces.

Based on hydrodynamics considerations, the flow field is significantly influenced by the present insert blockage and the secondary flow circulation. The insert increases the wetted perimeter and reduced the flow cross-section area. Figure 7 shows the unnoticeable buoyancy effects on the local Nusselt number in the entrance region of a horizontal tube with strip type insert with $AR = 1$ at different heat flux levels. From then on *Nu* decreases uniformly as it behaves in pure convection. Comparing with Fig. 6 for a bare tube, tubes with inserts strongly suggest that a mixed convection effect seems small. This again indicates that the buoyancy effects are dominant at $x/D \leqslant 20$ especially for the bare tube at a higher Q and lower Re (e.g. $Re = 6500$). In addition, the enhanced heat transfer effect shown in Fig. 7 is clearly noted and it is found that the value of enhanced heat transfer increases as Re decreases. This situation persists for tubes with LS and CS inserts (not shown here). The thermally entrance length in a tube with LS insert and $AR = 1$ was found about $4D$ in Fig. 7, which is smaller than that for a bare tube. The corresponding figures of Fig. 7 for LS and CS insert with $AR = 4$ are shown in Figs 8 and 9. Again, it is shown that the buoyancy effect seems negligible which is quite different from those from a bare tube due to a possible higher mixing resulting in a forced convection dominance caused by the present insert geometry ($AR = 4$). Overall, the Nusselt number distribution still behaves like a mixed convection environment with negligibly small buoyancy for LS and CS insert with $AR = 4$. The enhanced effect for these types of inserts in this study was found 1.5–2.8 times of the values for bare tubes by observing Figs 7–9.

The length-averaged Nusselt number was defined as:

$$\overline{Nu} = \frac{\bar{h}D}{k} = \left(\frac{Q_{\text{net}}}{\pi D \ell}\right)\left(\frac{1}{\ell}\int_0^{\ell} \frac{\mathrm{d}x}{T_{w,x} - T_{b,x}}\right)\left(\frac{D}{k}\right) \quad (4)$$

where $Q_{\text{net}} = mC_p(T_{bo} - T_{bi})$. The local values of the

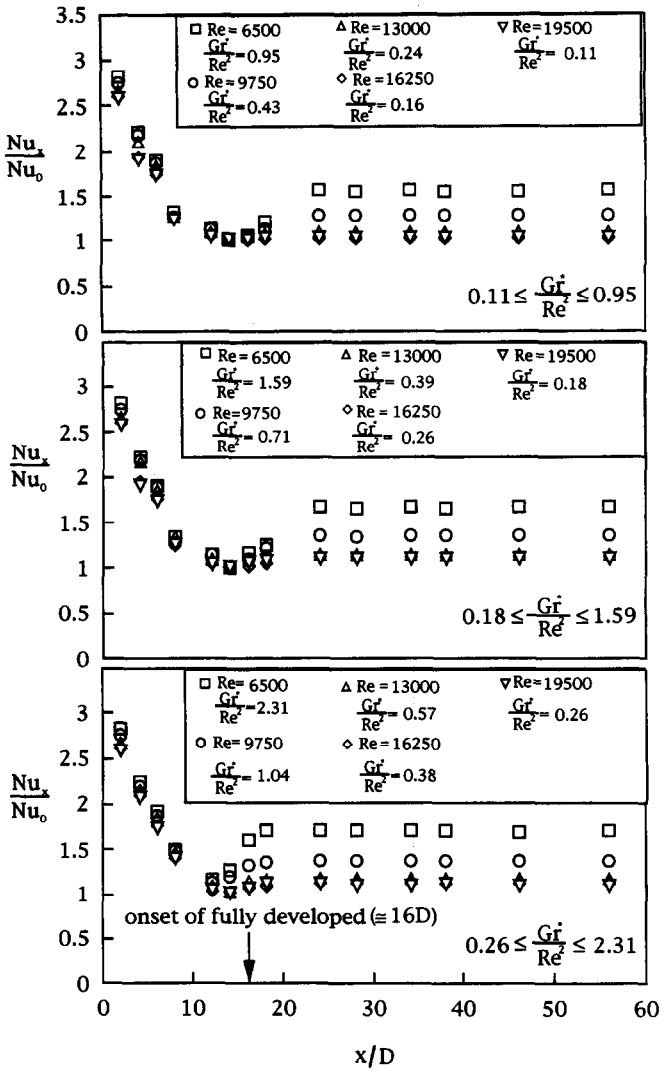

Fig. 6. Nu_x/Nu_0 vs x/D at different heat flux for bare tube.

thermophysical properties of air were obtained at a reference fluid temperature of $T_f = 0.5(T_{in} + T_{out})$. Figure 10 shows the data and the five correlations (bare tube and tubes with inserts) for the average Nusselt number plotted against Gr^*/Re^2. However, it is shown that the tube with insert usually has a better heat transfer rate than the one without insert. It strongly displays that LS insert with $AR = 1$ has the best heat transfer performance, followed by CS insert with $AR = 4$ and 5, and LS with $AR = 4$. The thermal buoyancy effect was also examined. The slope of the average Nusselt number curve in Fig. 10 indicates the influence of the parameter of Gr^*/Re^2. It is found that the buoyancy effect has a relatively little influence in tube with insert as one can see from the magnitude of exponent for Gr^*/Re^2 especially for LS insert with $AR = 1$ when $Gr^*/Re^2 \leqslant 0.004$.

A composite correlation of the experimental heat transfer data for all the tubes with inserts with different Gr^*/Re^2, and D/ℓ was formulated. All of the experimental data were then plotted in Fig. 11 and correlated with the equation which was also shown in Fig. 11. The equation shown in Fig. 10 is valid for air flow with Reynolds number in the range $6500 \leqslant Re \leqslant 19{,}500$, $5.82 \times 10^4 \leqslant Gr^* \leqslant 9.78 \times 10^7$ ($1.53 \times 10^{-4} \leqslant Gr^*/Re^2 \leqslant 2.31$), and $3.18 \times 10^{-3} \leqslant D/\ell \leqslant 6.57 \times 10^{-3}$. The empirical correlation predicts the experimental data with an average error of 2.45% and a maximum error 3.79%.

Nusselt number data for mixed convection from the present study are plotted in Fig. 12 as a function of Gr^* for Reynolds number 6500, 9750, 13,000, 16,250 and 19,500 to illustrate the effects of a wide range of this parameter. This plot was redrawn from [6] with several slight modifications for adding pure forced and natural convection data. The natural convection results were obtained when shut off the power supply for driven motor. Consequently, the forced con-

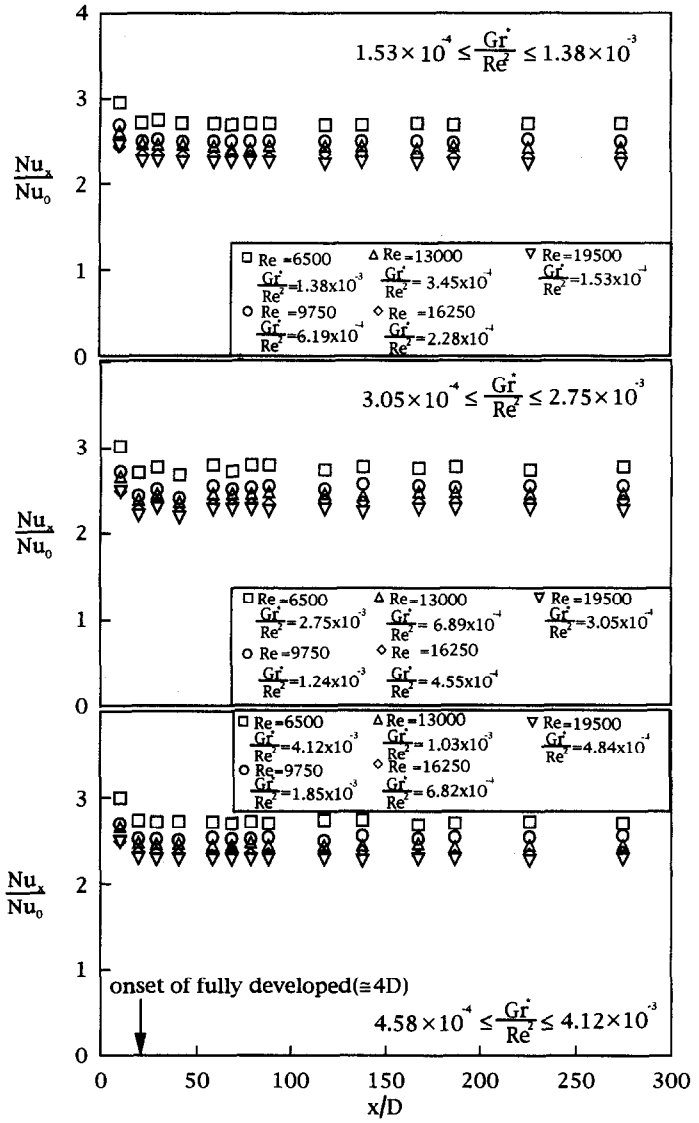

Fig. 7. Nu_x/Nu_0 vs x/D for LS insert with $AR = 1$ at different heat flux level.

vection results were secured from the following relation [10]:

$$Nu_F = (Nu_m^3 - Nu_N^3)^{\frac{1}{3}}. \quad (5)$$

Regardless of the Reynolds number forced convection Nu data calculated from Dittus Boelter correlation [9] also lie on the ordinate at $Gr^* = 0$ with a lower value than the corresponding one obtained from the experiments in Fig. 12, and pure natural convection values are located at bottom of each collection of data. Mixed convection data are located much higher than the natural convection. As the Reynolds number decreases, Nu data are located at smaller values of Gr^*, and spread over a smaller portion of the graph over a smaller range of Gr^*. After then, the increasing rate approaches a plateau. This situation becomes moderate as Re increases for bare tube. This is quite similar to the laminar results of Ligrani and Choi [11]. However, this behavior no longer exists for tube with inserts which can be seen in Fig. 12(b).

CONCLUSIONS

Developing turbulent mixed convection in a horizontal circular tube with strip-type inserts was extensively studied in the range of $1.53\times10^{-4} \leqslant Gr^*/Re^2 \leqslant 2.31$. The major conclusion can be drawn as follows:

(1) Systematic experimental data for steady-state mixed convection heat transfer are obtained and they were correlated in terms of Gr^*/Re^2 and D/ℓ and shown in Figs 10 and 11 for tubes with LS and CS inserts.

(2) The effect of the secondary flow and the aug-

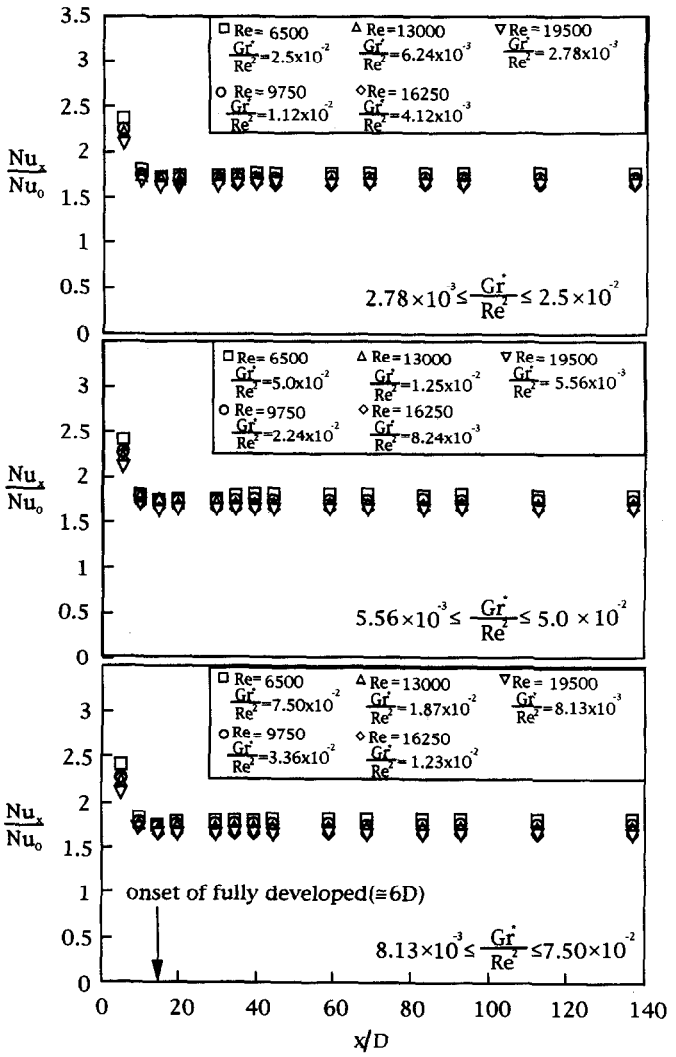

Fig. 8. Nu_x/Nu_0 vs x/D for LS insert with $AR = 4$ at different heat flux level.

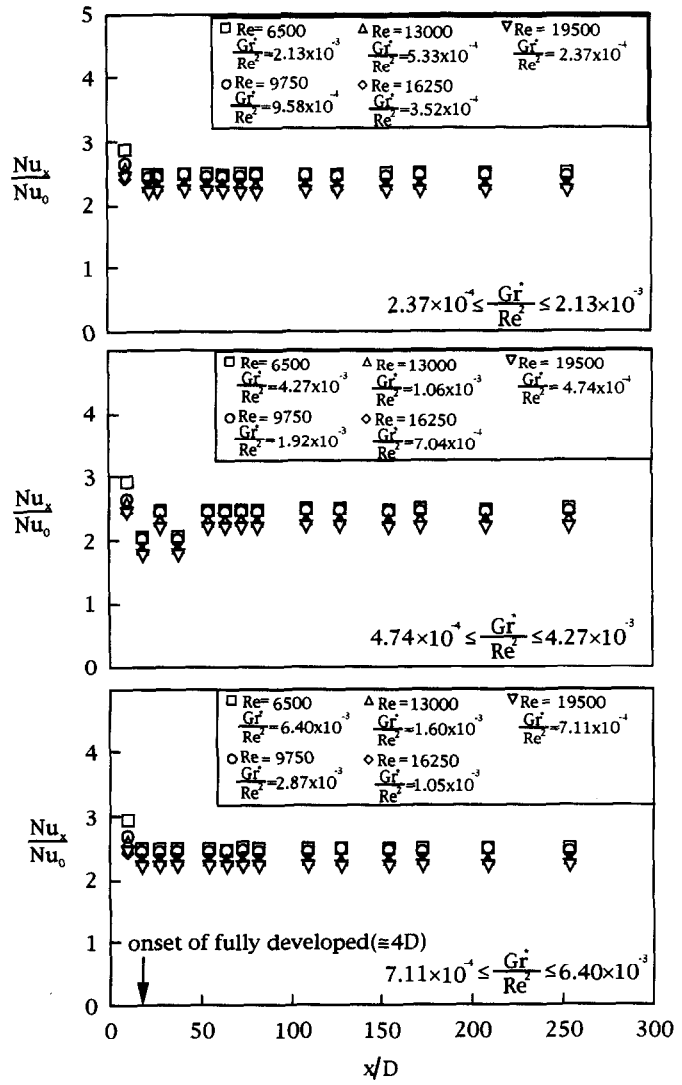

Fig. 9. Nu_x/Nu_0 vs x/D for CS insert with $AR = 4$ at different heat flux level.

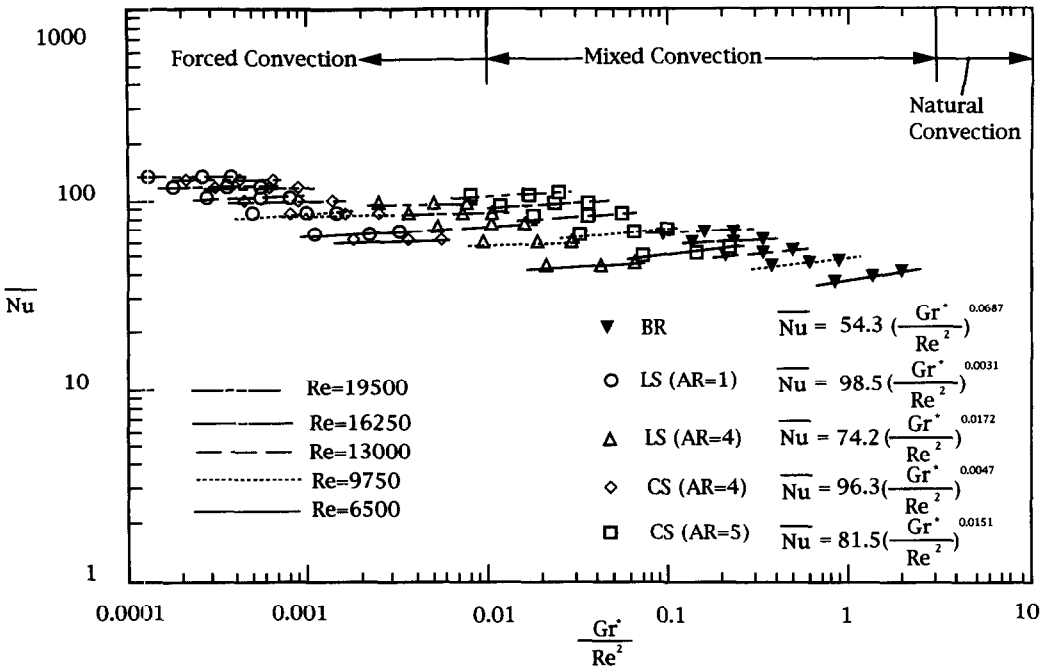

Fig. 10. $\overline{Nu}$ vs Gr^*/Re^2 at Re = 6500, 9750, 13,000, 16,250 and 19,500.

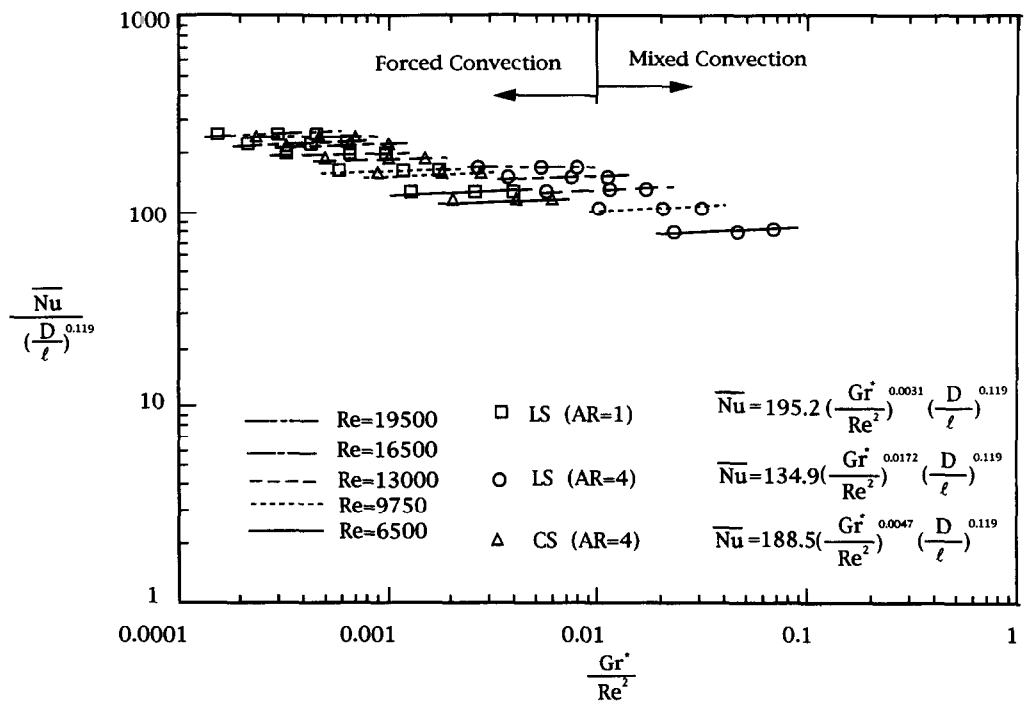

Fig. 11. The relationship of $\overline{Nu}$, Gr^*/Re^2 and D/ℓ.

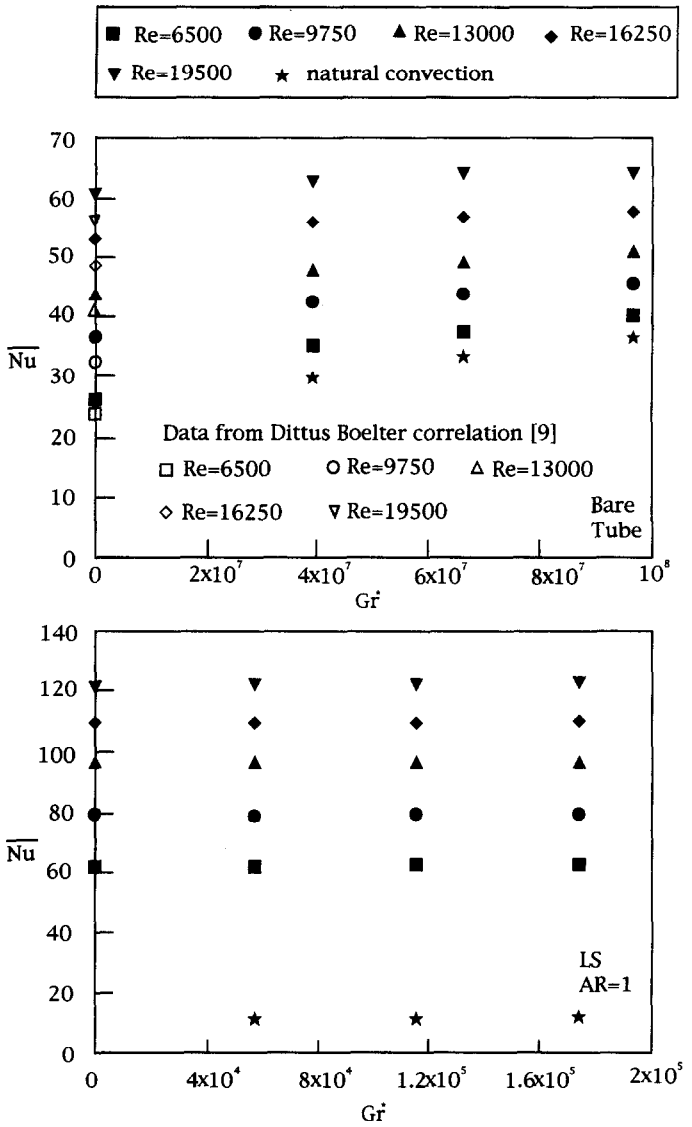

Fig. 12. Buoyancy effects on heat transfer in a horizontal circular tube with (LS, $AR = 1$)/without insert.

menting main flow direction buoyancy force has been found to be significant for the tube without insert at $Re = 6500$. However, with insert in the tube, the buoyancy effect could be negligible even at $Re = 6500$.

(3) The enhanced effect could be up to 2–3 times compared to the bare tube for the cases under study. It is found that LS with $AR = 1$ has the best thermal performance and the least influence of buoyancy effect.

REFERENCES

1. Shah, R. K. and Bhatti, M. S., Laminar convection heat transfer in ducts. In *Handbook of Single-Phase Convection Heat Transfer*, ed. S. Kakac, R. K. Shah and W. Aung. Chapter 3. Wiley, New York, 1987.
2. Solanki, S. C., Saini, J. S. and Gupta, D. P., An experimental investigation of fully developed laminar flow in a non-circular annulus. *Eighth National Conference on Heat Mass Transfer*, HMTA34-85, Visakhapatnam, 1985.
3. Solanki, S. C., Prakash, S., Saini, J. S. and Gupta, C. P., Forced convection heat transfer in doubly connected ducts. *International Journal of Heat Fluid Flow*, 1987, **8**, 107–110.
4. Chen, J.-D. and Hsieh, S.-S., Assessment study of longitudinal rectangular plate inserts as tubeside heat transfer augmentative device. *International Journal of Heat and Mass Transfer*, 1991, **34**, 2545–2553.
5. Hsieh, S.-S. and Wen, M.-Y., Developing three-dimensional laminar mixed convection in a circular tube inserted with longitudinal strips. *International Journal of Heat and Mass Transfer*, 1996, **39**, 299–310.
6. Liu, M.-H., Turbulent heat transfer and flow characteristics in a horizontal circular tube with strip-type inserts, Part II—heat transfer. MS thesis, Department of Mechanical Engineering, National Sun Yat-Sen University, 1996.

7. Moffat, R.-J., Describing the uncertainty in experimental results. *Experimental Thermal and Fluid Science*, 1988, **1**, 3–17.
8. Choi, D.-K. and Choi, D.-H., Developing mixed convection flow in a horizontal tube under circumferentially non-uniform heating. *International Journal of Heat and Mass Transfer*, 1994, **37**, 1899–1913.
9. Dittus, F.-W. and Boelter, M. K., University of California (Berkeley) Publication, 1930, Vol. 2, p. 443.
10. White, F. M., *Heat and Mass Transfer*. Addison-Wesley, New York, 1988, p. 415.
11. Ligrani, P.-H. and Choi, S., Mixed convection in straight and curved channels with buoyancy orthogonal to the forced flow. *International Journal of Heat and Mass Transfer*, 1996, **39**, 2473–2484.